# Multipolar polarizations of methane from isotropic and anisotropic collision-induced light scattering

T. Bancewicz,[1] K. Nowicka,[1] J.-L. Godet,[2] and Y. Le Duff[2]
[1]*Nonlinear Optics Division, Faculty of Physics, Adam Mickiewicz University, Umultowska 85, 61-614 Poznań, Poland*
[2]*Laboratoire des Propriétés Optiques des Matériaux et Applications, Université d'Angers, 2 boulevard Lavoisier, 49045 Angers, France*
(Received 22 January 2004; published 7 June 2004)

The anisotropic and isotropic binary collision-induced spectra scattered by gaseous methane have been measured in absolute units up to 900 $cm^{-1}$ from the Rayleigh line. Corresponding theoretical intensities taking into account multipolar polarizabilities have been calculated using a semiclassical procedure. From the analysis of, mainly, our isotropic scattering data, values of the dipole-quadrupole and dipole-octopole polarizabilities are deduced. They are found to be in good agreement with recent *ab initio* calculations.

DOI: 10.1103/PhysRevA.69.062704 PACS number(s): 34.50.−s, 33.20.Fb, 33.15.Kr, 33.70.−w

## I. INTRODUCTION

Molecular interactions are known to influence the scattering spectra of molecules. Generally, contributions of interaction-induced effects to scattering intensities generated by a gaseous sample depend on the symmetry of the particles involved [1,2]. For tetrahedral ($T_d$ symmetry) molecules, there are no functions that are invariant under the symmetry operations of $T_d$ in the subspaces of the first ($l=1$) and second ($l=2$) order connected to the spherical harmonics $\mathbf{Y}_l$ which describe molecular properties [3]. Then, for these molecules, the dipolar- and quadrupolar-type tensorial physical properties vanish and their dipole-dipole polarizability $\alpha$ is isotropic. The first source of anisotropy for the physical properties of tetrahedral symmetry molecules comes from third-rank tensors. Taking into account the linear response of that system to the applied field, the anisotropy mainly comes from the dipole-quadrupole (dipole-field gradient) polarizability $A_{\alpha,\beta\gamma}$. Thus, due to the isotropic nature of the dipole polarizability of the $CH_4$ molecule the light scattered by $CH_4$ monomers in the Rayleigh band is completely polarized. In consequence, the depolarized light signals in the Rayleigh wings are of purely interaction nature. Several studies of $CH_4$ collision-induced light scattering (CILS) spectra have been published [4,5]. They all concerned the anisotropic scattering spectra of $CH_4$ between 0 $cm^{-1}$ and 550 $cm^{-1}$. In these conditions, a relatively strong contribution of long-range interactions mainly identified as the dipole–induced-dipole (DID) effect is present and complicates the evaluation of contributions due to high-order multipolar polarizabilities.

In this paper we deduce the multipolar polarizabilities of $CH_4$ molecules from light scattering (CILS) spectroscopy studying as well the anisotropic and isotropic Rayleigh wings of gaseous methane up to a frequency shift $\nu$ of 900 $cm^{-1}$. We shall show that the *isotropic* CILS spectrum of $CH_4$ samples is very suitable to study high-order polarizabilities. Indeed in the case of the isotropic CILS spectrum of $CH_4$, the DID interaction contributes only to the second order, giving us a good opportunity to study multipolar polarizabilities, the **A** tensor in particular. The dipole-octopole (dipole gradient of the field gradient) polarizability $E_{\alpha,\beta\gamma\delta}$ is also investigated. A comparison of experimental data with computed theoretical intensities calculated using *ab initio* polarizabilities recently obtained is made.

## II. THEORY

In a dense medium, collisional effects as well as time and space fluctuations of multipolar molecular fields will in general lead to changes in the pair polarizability tensor. For tetrahedral molecules, in a first approximation, the long-range field-induced change in the pair polarizability related to the linear multipolar polarizabilities reads (up to the octopole-induced octopole light scattering mechanism) [6]

$$\begin{aligned}\Delta\mathbf{A} = (1+\mathcal{P}_{AB})\Big\{ & \alpha_0^2\mathbf{T}_2^{(AB)} + \frac{1}{3}\alpha_0(\mathbf{A}_A^{(1,2)}[2]\mathbf{T}_3^{(AB)} - \mathbf{T}_3^{(AB)} \\ & \times[2]\mathbf{A}_B^{(2,1)}) + \frac{1}{15}\alpha_0(\mathbf{A}_A^{(1,3)}[3]\mathbf{T}_4^{(AB)} + \mathbf{T}_4^{(AB)}[3]\mathbf{A}_B^{(3,1)}) \\ & + \frac{1}{9}\mathbf{A}_A^{(1,2)}[2]\mathbf{T}_4^{(AB)}[2]\mathbf{A}_B^{(2,1)} + \frac{1}{45}(\mathbf{A}_A^{(1,2)}[2]\mathbf{T}_5^{(AB)}[3]\mathbf{A}_B^{(3,1)} \\ & - \mathbf{A}_A^{(1,3)}[3]\mathbf{T}_5^{(AB)}[2]\mathbf{A}_B^{(2,1)}) + \frac{1}{225}\mathbf{A}_A^{(1,3)}[3]\mathbf{T}_6^{(AB)}[3]\mathbf{A}_A^{(3,1)} \\ & + \cdots\Big\}, \end{aligned} \tag{1}$$

where $\alpha_0$ is the dipole polarizability whereas the tensor $\mathbf{A}_i^{(1,m)}$ of rank $1+m$ determines the linear-dipole $m$th-rank multipole polarizability due to electric-dipole–$2^{**}m$-pole transitions in a molecule $i$. The symbol $[m]$ denotes $m$-fold contraction whereas $\mathcal{P}_{AB}$ permutes the indices $A$ and $B$. Moreover, $\mathbf{T}_N^{(AB)}=(\nabla)^N(1/R_{AB})$ stands for the intermolecular interaction tensor. Usually in the literature the following brief notation for, respectively, the dipole-quadrupole and the dipole-octopole polarizability, $\mathbf{A}^{(1,2)}=\mathbf{A}, \mathbf{A}^{(1,3)}=\mathbf{E}$, is used. We note that for tetrahedral molecules **A** is the leading anisotropic polarizability. This polarizability gives the main contribution to the collision-induced rotational Raman (CIRR) scattering [7] considered here. The irreducible spherical version of Eq. (1) has been derived elsewhere [8]. In Table I we give for tetrahedral molecules the form of the

 

TABLE I. Excess multipolar-origin pair polarizability $\Delta A_{KM}$ due to the **A** tensor: isotropic ($K=0$) and anisotropic ($K=2$) cases.

| Mechanism | $j_A$ | $j_B$ | $l_A$ | $l_B$ | $N$ | $\Delta A_{00}$ | $\Delta A_{2M}$ |
|---|---|---|---|---|---|---|---|
| $\alpha\mathbf{T}_3\mathbf{A}$ | 0 | 3 | 1 | 2 | 3 | $(\sqrt{14}/3)\Lambda_{00}$ | $(2\sqrt{7/3}/5)\Lambda_{2M}$ |
| $\mathbf{AT}_4\mathbf{A}$ | 3 | 3 | 2 | 2 | 4 | $(-\sqrt{11/15}/3)\Xi^{(4)}_{00}$ | $\Sigma_{x=2}^{6}\, a_x\Xi^{(x)}_{2M}$ |
| $\mathbf{AT}_5\mathbf{E}$ | 3 | 4 | 2 | 3 | 5 | $(\sqrt{143/14}/45)\Xi^{(5)}_{00}$ | $\Sigma_{x=3}^{7}\, b_x\Xi^{(x)}_{2M}$ |

$$\Lambda_{KM}={}_{(A)}\alpha_0\{\mathbf{T}_3^{(AB)}\otimes{}_{(B)}\mathbf{A}_3^{(1,2)}\}_{KM}-{}_{(B)}\alpha_0\{\mathbf{T}_3^{(AB)}\otimes{}_{(A)}\mathbf{A}_3^{(1,2)}\}_{KM}$$

$$\Xi^{(x)}_{KM}=\{\mathbf{T}_N^{(AB)}\otimes[{}_{(A)}\mathbf{A}_{j_A}^{(1,l_A)}\otimes{}_{(B)}\mathbf{A}_{j_B}^{(1,l_B)}]_{(x)}\}_{KM}$$

$$a_2=-\sqrt{2/35}/15,\ a_3=0, a_4=\sqrt{2/105}/3,\ a_5=0,\ a_6=-\sqrt{13/5}/3$$

$$b_3=1/30\sqrt{105},\ b_4=-1/150\sqrt{7},\ b_5=-\sqrt{11/42}/50,\ b_6=\sqrt{13/10}/90,\ b_7=1/3\sqrt{5}$$

excess multipolar isotropic and anisotropic pair polarizability due to the **A** tensor. For tetrahedral molecules the **E** tensor contribution to the pair polarizability is of the same form as that for octahedral molecules. For the **E** tensor contribution, see Ref. [9].

Multipolar polarizabilities can be given in Cartesian and in spherical coordinates. The dynamic- or frequency-dependent multipolarizabilities are in general complex. The dynamic reducible spherical polarizability $A^{m_1m_2}_{l_1l_2}(\omega)$ is given by [10,11]

$$A^{m_1m_2}_{l_1l_2}(\omega)=2\hbar^{-1}\sum_{n\neq 0}Z(\omega,\omega_{n0},\Gamma_{n0})[\omega_{n0}\mathrm{Re}\{\langle 0|Q^{m_1}_{l_1}|n\rangle \times\langle n|Q^{m_2}_{l_2}|0\rangle\}+i\omega\ \mathrm{Im}\{\langle 0|Q^{m_1}_{l_1}|n\rangle\langle n|Q^{m_2}_{l_2}|0\rangle\}], \tag{2}$$

where $Q^m_l$ is the $m$th component of the spherical multipole moment tensor of order $l$ and the complex function $Z(\omega,\omega_{n0},\Gamma_{n0})$ is composed of the dispersion function $f$ and the absorption function $g$:

$$Z(\omega,\omega_{n0},\Gamma_{n0})=f(\omega,\omega_{n0},\Gamma_{n0})+ig(\omega,\omega_{n0},\Gamma_{n0}). \tag{3}$$

In the static (zero-frequency) limit, Eq. (2) reduces to

$$A^{m_1m_2}_{l_1\ l_2}=2\sum_{n\neq 0}\frac{\langle 0|Q^{m_1}_{l_1}|n\rangle\langle n|Q^{m_2}_{l_2}|0\rangle}{E_n-E_0}. \tag{4}$$

The reducible tensor $A^{m_1m_2}_{l_1\ \ l_2}$ can be decomposed into irreducible parts $A_{jm}[l_1l_2]$ by

$$A_{jm}[l_1l_2]=\sum_{m_1,m_2}C(l_1,l_2,j;m_1,m_2,m)A^{m_1m_2}_{l_1l_2}, \tag{5}$$

where $C(l_1,l_2,j;m_1,m_2,m)$ stands for the Clebsch-Gordan coefficient.

A general dipole-quadrupole polarizability $A_{\alpha,\beta\gamma}$(DQ) tensor has $3^3=27$ components. Taking into account that the quadrupole moment is traceless and symmetric to its indices, we can write 12 equations connecting the $A_{\alpha,\beta\gamma}$ components. Finally the **A** tensor has 15 independent elements. The number of its independent elements is clearly visible from the reducible spherical form $A^{m_1m_2}_{1\ 2}(3\times 5=15)$. For $CH_4$, the tetrahedral symmetry molecule considered here (the $T_d$ point symmetry group), the dipole-quadrupole polarizability **A** tensor has six nonzero elements but only *one independent* component: $A_{x,yz}=A_{x,zy}=A_{y,xz}=A_{y,zx}=A_{z,xy}=A_{z,yx}\equiv A$ [10]. In our considerations we assume a coordinate system with the C atom in its center and H molecules at the positions $(1,1,1)$, $(-1,-1,1)$, $(-1,1,-1)$, $(1,-1,-1)$. To discuss this tensor in spherical coordinates the projection operator technique is very useful [12]. Using the projection operator for tetrahedral symmetry we find the following linear combination of reducible spherical dipole-quadrupole $A^{m_1m_2}_{1\ 2}$ polarizability tensor components transforming according to the totally symmetric representation of the molecular point group $T_d$:

$$A^{0-2}_{12}+\sqrt{2}A^{-1-1}_{12}-\sqrt{2}A^{11}_{12}-A^{02}_{12}. \tag{6}$$

The above formula allows us to find the following relative values of $A^{m_1m_2}_{12}$:

$$A^{0-2}_{12}:A^{02}_{12}:A^{-1-1}_{12}:A^{11}_{12}=1:-1:\sqrt{2}:-\sqrt{2}. \tag{7}$$

Moreover, taking the definition of $\mu^0_1=\mu_z$ and $Q^{-2}_2=(1/\sqrt{6})(Q_{xx}+Q_{yy}-2iQ_{xy})$ [11] we find that

$$A^{0-2}_{12}=-i\sqrt{\frac{2}{3}}A. \tag{8}$$

Then, using Eqs. (5), (7), and (8) for the spherical irreducible form of the dipole-quadrupole polarizability tensor we obtain

$$A_{32}[12]=-A_{3-2}[12]=i\sqrt{2}A. \tag{9}$$

A general dipole-octopole (DO) polarizability $E_{\alpha,\beta\gamma\delta}$ tensor has $3^4=81$ components. The number of its independent elements is clearly visible from the reducible spherical form $A^{m_1m_2}_{13}(3\times 7=21)$. For the tetrahedral symmetry molecule there are 21 nonzero elements for this tensor but there is only one independent component [13]. We select the $E_{z,zzz}$ component for our considerations here. Similarly to the case of the **A** tensor using the projection operator we find the following relative values of $A^{m_1m_3}_{13}$:

$$A^{00}_{13}:A^{13}_{13}:A^{-1-3}_{13}:A^{-11}_{13}:A^{1-1}_{13}=1:\sqrt{\frac{3}{8}}:\sqrt{\frac{3}{8}}:\frac{\sqrt{10}}{4}:\frac{\sqrt{10}}{4}. \tag{10}$$

Moreover, we can easily show that

TABLE II. Excess anisotropic *nonlinear origin* pair polarizability $\Delta A_{2M}^{(NL)}$.

| Mechanism | $j_A$ | $l_A$ | $l_B$ | N | $\Delta A_{2M}^{(NL)}$ |
|---|---|---|---|---|---|
| $\mathbf{B}_0\mathbf{T}_5\ \mathbf{\Omega}$ | 0 | 2 | 3 | 5 | $\sqrt{11/15}/30[\{\mathbf{T}_5^{(AB)}\otimes[{}_{(A)}\mathbf{B}_0\otimes{}_{(B)}\mathbf{\Omega}_3]_{(3)}\}_{2M}-\{\mathbf{T}_5^{(AB)}\otimes[{}_{(A)}\mathbf{\Omega}_3\otimes{}_{(B)}\mathbf{B}_0]_{(3)}\}_{2M}]$ |
| $\mathbf{bT}_4\ \mathbf{\Omega}$ | 3 | 1 | 3 | 4 | $\Sigma_x\ b_x[\{\mathbf{T}_4^{(AB)}\otimes[{}_{(A)}\mathbf{b}_3\otimes{}_{(B)}\mathbf{\Omega}_3]_{(x)}\}_{2M}+(-1)^x\{\mathbf{T}_4^{(AB)}\otimes[{}_{(A)}\mathbf{\Omega}_3\otimes{}_{(B)}\mathbf{b}_3]_{(x)}\}_{2M}]$ $b_2=1/30\sqrt{7}\quad b_3=1/30\quad b_4=\sqrt{3/7}/10\ b_5=\sqrt{11}/30\quad b_6=\sqrt{13/2}/15$ |
| $\mathbf{bT}_5\ \mathbf{\Phi}$ | 3 | 1 | 4 | 5 | $\Sigma_x b_x[\{\mathbf{T}_5^{(AB)}\otimes[{}_{(A)}\mathbf{b}_3\otimes{}_{(B)}\mathbf{\Phi}_4]_{(x)}\}_{2M}+(-1)^x\{\mathbf{T}_5^{(AB)}\otimes[{}_{(A)}\mathbf{\Phi}_4\otimes{}_{(B)}\mathbf{b}_3]_{(x)}\}_{2M}]$ $b_3=-1/90\sqrt{10}\quad b_4=-1/50\sqrt{6}\quad b_5=-\sqrt{11}/225\ b_6=-\sqrt{13/105}/15\quad b_7=-1/2\sqrt{210}$ |
| $\mathbf{B}_4\mathbf{T}_5\ \mathbf{\Omega}$ | 4 | 2 | 3 | 5 | $\Sigma_x b_x[\{\mathbf{T}_5^{(AB)}\otimes[{}_{(A)}\mathbf{B}_4\otimes{}_{(B)}\mathbf{\Omega}_3]_{(x)}\}_{2M}+(-1)^x\{\mathbf{T}_5^{(AB)}\otimes[{}_{(A)}\mathbf{\Omega}_3\otimes{}_{(B)}\mathbf{B}_4]_{(x)}\}_{2M}]$ $b_3=1/60\sqrt{105}\quad b_4=1/60\sqrt{7}\quad b_5=\sqrt{11/42}/30\quad b_6=\sqrt{13/10}/30\quad b_7=1/6\sqrt{5}$ |

$$A_{13}^{00}=E_{z,zzz}\equiv E. \tag{11}$$

Then, using Eqs. (5), (10), and (11) for the spherical irreducible form of the dipole-octopole polarizability tensor we obtain

$$A_{40}[13]=\frac{\sqrt{7}}{2}E, \tag{12}$$

$$A_{4\pm4}[13]=\frac{1}{2}\sqrt{\frac{5}{2}}E. \tag{13}$$

The additional variation in the pair polarizability results from nonlinear molecular polarizabilities combined with its permanent multipoles [14–16]. For $CH_4$ we consider the dipole hyperpolarizability **b** combined with the permanent octopole moment $\mathbf{\Omega}$ and the dipole$^2$-quadrupole hyperpolarizability **B** combined with the permanent hexadecapole $\mathbf{\Phi}$. Using similar arguments to those given above for **A** and **E** tensors we show that for the dipole$^2$-quadrupole hyperpolarizability tensor $B_{\alpha,\beta,\gamma\delta}$ the following relations between its irreducible spherical and Cartesian components hold [17]:

$$B_{00}[(11)22]=\sqrt{\frac{6}{5}}B_0,$$

$$B_{40}[(11)22]=\frac{\sqrt{\frac{7}{15}}}{2}\Delta B,\quad B_{4\pm4}[(11)22]=\frac{\Delta B}{2\sqrt{6}}, \tag{14}$$

where $B_0=B_{z,z,zz}+2B_{x,z,xz}$ and $\Delta B=3B_{z,z,zz}-4B_{x,z,xz}$ whereas for the dipole$^3$ hyperpolarizability tensor $b_{\alpha\beta\gamma}$ we obtain

$$b_{3\pm2}[(11)21]=\pm i\sqrt{2}b, \tag{15}$$

where $b=b_{xyz}$. For the first not vanishing octopole $Q_{3\pm2}$ and hexadecapole $Q_{40}$ and $Q_{4\pm4}$ multipole moments of $CH_4$ molecule, see [3,11,17].

Table II gives the tetrahedral molecules form of the excess Rayleigh *nonlinear origin* pair polarizability due to the **b** tensor. For tetrahedral molecules the **B** tensor contribution to the pair polarizability is of the same form as that for octahedral molecules. For the **B** tensor contribution, see [17].

Now let us consider a macroscopically isotropic system composed of *N*-like globular molecules in an active scattering volume *V* illuminated by laser radiation of the angular frequency $\omega_L=2\pi\nu_L$, polarized linearly in the direction **e**. We analyze the secondary electromagnetic radiation emitted by the system in response to that perturbation. At a point **R** distant from the center of the sample, the radiation scattered at $\omega_s=2\pi(\nu_L-\nu)$ is measured on traversal of an analyzer with polarization **n**. Then the quantum-mechanical expression for the pair differential scattering cross section has the form [18]

$$V\left(\frac{\partial^2\sigma}{\partial\omega\,\partial\Omega}\right)=\frac{\omega_s^4}{c^4}\frac{1}{2\pi}\int_{-\infty}^{\infty}dt\ e^{-i\omega t}\underbrace{\langle(\mathbf{n}\cdot\Delta\mathbf{A}(0)\cdot\mathbf{e})(\mathbf{n}\cdot\Delta\mathbf{A}(t)\cdot\mathbf{e})\rangle}_{F(t)}. \tag{16}$$

The isotropic $I_{iso}(\nu)$ and anisotropic $I_{ani}(\nu)$ collision-induced light scattering intensities being expressed as a pair of double differential cross sections, we obtain

$$I_{iso}(\nu)=\frac{(\mathbf{e}\cdot\mathbf{n})^2}{3}\frac{\omega_s^4}{c^4}\frac{1}{2\pi}\int_{-\infty}^{\infty}dt\ e^{-i2\pi\nu t}F_{00}(t), \tag{17}$$

$$I_{ani}(\nu)=\frac{3+(\mathbf{e}\cdot\mathbf{n})^2}{30}\frac{\omega_s^4}{c^4}\frac{1}{2\pi}\int_{-\infty}^{\infty}dt\ e^{-i2\pi\nu t}F_{22}(t), \tag{18}$$

where

$$F_{KK}(t)=\langle\Delta\mathbf{A}_{(K)}(0)\odot\Delta\mathbf{A}_{(K)}(t)\rangle. \tag{19}$$

The subsequent correlation functions $F_{00}(t)$ and $F_{22}(t)$ may be written in the form [19]

$$F_{KK}^{(NL)}(t) = \sum_{N,j_1,j_2 \geqslant j_1} \varphi_{KK}^{N,j_1,j_2} S_N(t) R_{j_1}(t) R_{j_2}(t), \qquad (20)$$

where the translational functions $S_N(t)$, the rotational functions $R_j(t)$, and the coefficients $\varphi_{KK}^{N,j_1,j_2}$ associated with the successive multipolar mechanisms or with the nonlinear origin mechanisms including $b$ and $\Delta B$ have been defined elsewhere [19]. The nonlinear origin coefficients due to $B_0$ are $\varphi_{22}^{5,0,3} = \frac{864}{25}\Omega^2 B_0^2$ and $\varphi_{22}^{6,0,4} = \frac{1584}{35}\Phi^2 B_0^2$. Let us underline that the nonlinear coefficients are related to the anisotropic spectrum only.

## III. EXPERIMENT

The scattering spectra reported in this work have been recorded using a 90° scattering experiment previously described [19]. We used the green line of an argon laser ($\lambda_L = 514.5$ nm) to illuminate gaseous samples contained in a four-window high-pressure cell. $CH_4$ gas was provided by L'Air Liquide company with impurities less than 5 ppm. Methane densities were deduced from pressure measurements and *P-V-T* data given in Ref. [20]. The light scattered by methane was analyzed by a double monochromator and detected using either a photomultiplier or a charge-coupled-device (CCD) camera cooled at 140 K [21]. Two types of scattering intensities were recorded: polarized intensities $I^{\perp}$ and depolarized intensities $I^{\parallel}$ according to the polarization of the laser beam, perpendicular or parallel, respectively, to the scattering plane [22]. At several frequencies the scattering intensities were measured at various densities $\rho$ up to 320 amagat. Then, for each studied frequency $\nu$, the pair intensity $I_2(\nu)$ was deduced as the coefficient proportional to the square density in the virial expansion given by

$$I^L(\nu) = I_0^L(\nu) + I_1^L(\nu)\rho + I_2^L(\nu)\rho^2 + I_3^L(\nu)\rho^3. \qquad (21)$$

The superscript $L$ stands for $\perp$ or $\parallel$ according to the laser polarization. The coefficients $I_0^L(\nu)$, $I_1^L(\nu)$, and $I_3^L(\nu)$ depend on the experimental setup and/or the studied sample [19]. To make easier the comparison between the CILS intensities recorded for different experimental conditions, $I^L(\nu)$ have been measured relative to $I_{\nu_1}^{\perp}$, the integrated intensity of the vibration Raman line $\nu_1$ of $CH_4$. Typical curves $I_{\nu}^{\parallel}/I_{\nu_1}^{\perp}$ are displayed in Fig. 1 for several frequency shifts $\nu$ (50 $cm^{-1}$, 100 $cm^{-1}$, 200 $cm^{-1}$, and 300 $cm^{-1}$). For each value of the Raman frequency $\nu$ studied, pair intensities $I_2^L(\nu)$ were obtained from the slope of these curves (see Fig. 1) at the zero-density limit. A spectral correction was applied for each recorded intensity to take into account the change of the sensitivity of our apparatus (double monochromator plus photodetector) with wavelength. Besides, since scattering intensities are obtained in a first step on a relative scale, a calibration has been made to put them on an absolute scale using the rotational $S_0(1)$ line of hydrogen as an external reference [23]. Thus we have obtained, on an absolute scale, the values $I_2^{\perp,a}(\nu)$ and $I_2^{\parallel,a}(\nu)$ of the polarized and depolarized intensities, respectively. Then the pair anisotropic CILS spectrum $I_{ani}(\nu)$ and the pair isotropic CILS spectrum $I_{iso}(\nu)$ were deduced from the equations

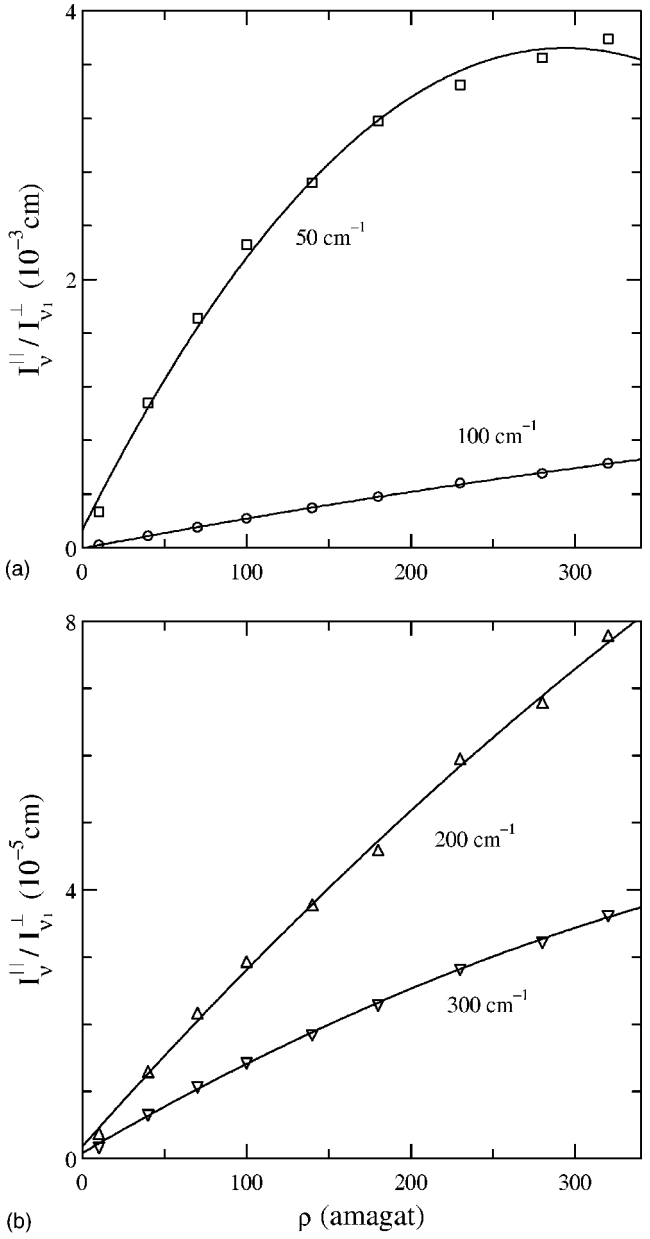


FIG. 1. Experimental CILS depolarized intensities $I_{\nu}^{\parallel}$ divided by the integrated intensity $I_{\nu_1}^{\perp}$ of the $\nu_1$ Raman line for gaseous $CH_4$ at 294.5 K and versus density $\rho$ (in amagats). The CILS intensities are measured at several frequency shifts: (a) 50 $cm^{-1}$ (□) and 100 $cm^{-1}$ (○); (b) 200 $cm^{-1}$ (△) and 300 $cm^{-1}$ (▽).

$$I_{ani}(\nu) = I_2^{\parallel,a}(\nu), \qquad (22)$$

$$I_{iso}(\nu) = I_2^{\perp,a}(\nu) - \frac{7}{6} I_2^{\parallel,a}(\nu). \qquad (23)$$

## IV. RESULTS AND DISCUSSION

The experimental depolarization ratio $\eta(\nu) = I_2^{\parallel}(\nu)/I_2^{\perp}(\nu)$ deduced from the measurement of the binary Rayleigh spectra $I_2^{\parallel}(\nu)$ and $I_2^{\perp}(\nu)$ at 294.5 K is presented in Fig. 2 versus frequency shift in $cm^{-1}$. It can be compared to the theoretical

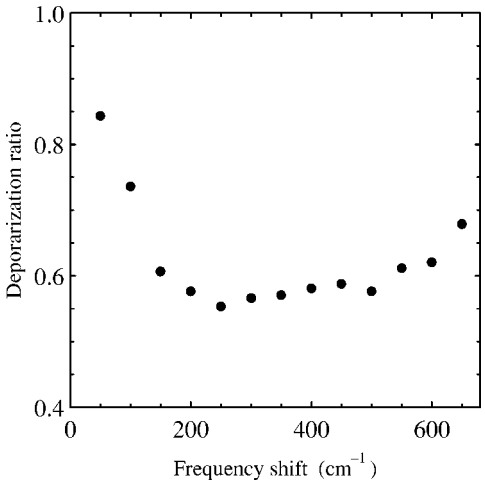


FIG. 2. Experimental pair depolarization ratio $\eta(\nu) = I_2^{\parallel}(\nu)/I_2^{\perp}(\nu)$ versus frequency shifts $\nu$ in cm$^{-1}$ for the two-body CIS of gaseous $CH_4$ at 294.5 K.

depolarization ratios associated with the dipole-induced dipole (DID), dipole-quadrupole (DQ), and dipole-octopole (DO) mechanisms: $\eta^{DID}=6/7\approx 0.87$, $\eta^{DQ}=9/23\approx 0.39$, and $\eta^{DO}=22/63\approx 0.35$, respectively [24]. The expected depolarization ratio for the first-order DID mechanism corresponds to completely depolarized scattered intensities. In Fig. 2, it appears that such a situation exists in the vicinity of the Rayleigh line. However, beyond 150 cm$^{-1}$, scattered intensities become more polarized and the experimental depolarization ratio is close to 0.6. This behavior shows that the DID interaction alone cannot generate the scattered intensities observed and that dipole-multipole mechanisms could contribute significantly at high-frequency shifts. Notice that in the frequency range where $\eta(\nu)$ is far lower than 6/7, the isotropic spectrum is defined with more accuracy [as can be deduced from Eq. (23)].

In Figs. 3 and 4, the experimental Rayleigh anisotropic and isotropic binary intensities scattered by gaseous $CH_4$ at 294.5 K are displayed, respectively, on an absolute scale (in cm$^6$) versus frequency shifs, together with their error bars. Both spectra have been recorded up to 900 cm$^{-1}$ from the Rayleigh line. Nevertheless, due to excessively large uncertainties, isotropic intensities must be considered just as estimations below 100 cm$^{-1}$ and beyond 650 cm$^{-1}$. Previous data concerning anisotropic collision-induced intensities published in Ref. [4] up to 550 cm$^{-1}$ are also provided in Fig. 3. They are in satisfactory agreement with our data. On the other hand, in Figs. 3 and 4, anisotropic and isotropic scattering theoretical intensities calculated by using a recent isotropic potential of $CH_4$ are also displayed. This isotropic potential has been obtained from a spherical harmonic expansion [25] of the potential computed by Palmer and Anchell (PA) [26]. Every theoretical spectrum takes into account the translational DID mechanism and rototranslational mechanisms [DQ, DO, cross terms including quadrupole-quadrupole, quadrupole-octopole, and octopole-octopole interactions (CT=QQ+QO+OO)]. The contribution of nonlinear polarizabilities to the anisotropic spectrum (NL) is also considered. The value of the dipole polarizability used for

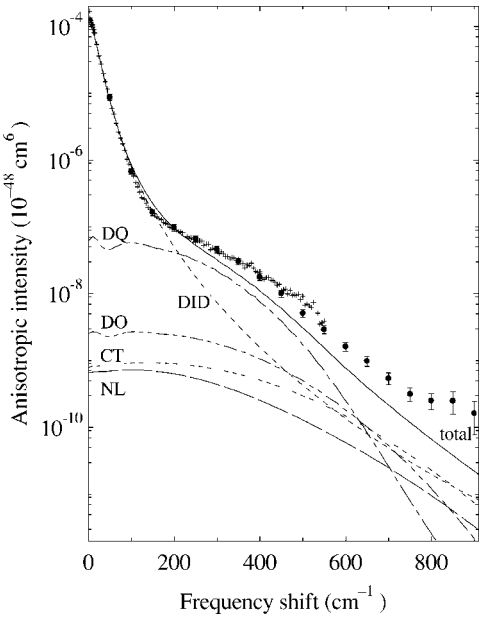


FIG. 3. Two-body *anisotropic* scattering spectra of $CH_4$ gas at 294.5 K. The solid circles (●) indicate our experimental data with error bars; crosses (+) are previous data from Ref. [4]. Curves are theoretical spectra computed by using the potential of Palmer and Anchell (PA) [26], the dipole polarizability $\alpha_0=2.642$ Å$^3$ [27], and the *ab initio* computed values of Maroulis ($A=0.71$ Å$^4$ and $E=0.78$ Å$^5$) [28]. The successive multipolar mechanisms are represented by - - - - (DID), — - — - (DQ), — - - — (DO), - - - - - - (CT), and — — (NL). The solid line (———) corresponds to the total theoretical spectrum.

calculations is $\alpha_0=2.642$ Å$^3$ [27]. For rototranslational and NL contributions, we use the *ab initio* values of the DQ polarizability *A* and of the DO polarizability *E* recommended by Maroulis [28] and reported in Table III. Hyperpolarizabilities and permanent multipoles playing a role in the reported NL contribution have also been computed by Maroulis [29].

Rototranslational and NL contributions result from convolution products of rotational stick spectra and translational broadening functions. This computation has been described elsewhere [19]. Concerning DID, computations of the classical trajectories of two molecules in interaction have been carried out by following the standard procedure [30], but for free dimers only. Indeed, knowledge of the complementary contribution of bound and metastable dimers (pairs of molecules trapped in the well of the effective potential) is not necessary. First, the percentages *x* of the isotropic and anisotropic integrated DID intensities due to bound and metastable dimers are low in the $CH_4$ case. Using the PA potential and the statistical method described by Levine [31], we found that $x_{iso}=15\%$ and $x_{ani}=13\%$. Second, the role of these low-energy pairs is limited to the low-frequency spectra ($\nu<25$ cm$^{-1}$) [4]. Therefore, calculation of their spectral contributions is not useful for an evaluation of the dipole-multipole polarizability tensors based on a comparison between theory and experiment beyond 100 cm$^{-1}$.

Three isotropic potentials $V(r)$ have been selected for calculations: a Lennard-Jones (LJ) one [32], the one of Righini-

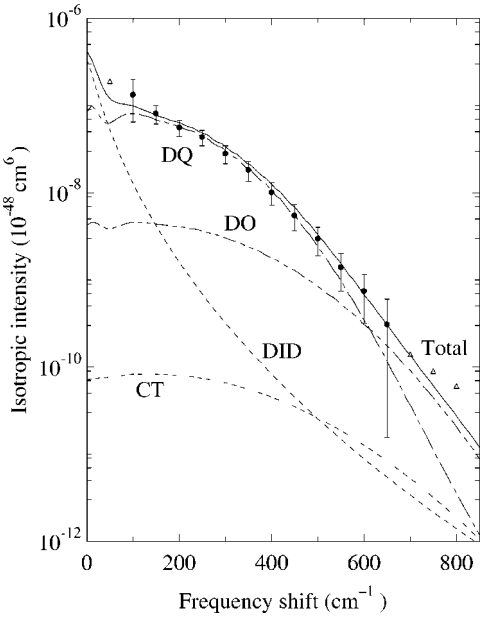


FIG. 4. Two-body *isotropic* scattering spectra of $CH_4$ gas at 294.5 K. The solid circles (●) indicate our experimental data with error bars; triangles (△) are estimated data. Curves are theoretical spectra computed by using the potential of Palmer and Anchell (PA) [26], the dipole polarizability $\alpha_0=2.642$ Å$^3$ [27], and the ab initio computed values of Maroulis ($A=0.71$ Å$^4$ and $E=0.78$ Å$^5$) [28]. The successive multipolar mechanisms are represented by - - - - (DID), — - — - (DQ), — - - — (DO), and - - - - - - (CT). The solid line (———) corresponds to the total theoretical spectrum.

Maki-Klein (RMK) modified by Meinander and Tabisz [33], and the aforementioned PA potential of Palmer and Anchell [26]. We checked that they generate theoretical intensities compatible with our measurements. In particular, the DID contribution to the anisotropic spectrum is responsible for most of the integrated intensity. Therefore, the theoretical zero-order moment $M_{0,\beta}^{th}$ associated with the DID anisotropy $\beta(r)=6\alpha_0^2/r^3$,

$$M_{0,\beta}^{th}=\int_0^\infty \beta(r)^2\exp[-V(r)/k_BT]4\pi r^2dr, \qquad (24)$$

must be close to the experimental zero-order moment $M_0^{ani}$ [1]:

$$M_0^{ani}=\frac{15}{2}\left(\frac{\lambda_L}{2\pi}\right)^4\int_{-\infty}^{\infty} I_{ani}(\nu)d\nu. \qquad (25)$$

Using the low-frequency intensities obtained by Barocchi *et al.* [4], we found that $M_0^{ani}=188\pm20$ Å$^9$. In previous works, Meinander *et al.* provided $M_0^{ani}=205\pm14$ Å$^9$ [27,34]. Both results are fully compatible with momenta generated by the LJ and PA potentials ($M_{0,\beta}^{th}=191$ and 200 Å$^9$, respectively). For RMK, we found a higher value ($M_{0,\beta}^{th}=225$ Å$^9$). Nevertheless, possible short-range effects may lessen this latter result and make the RMK potential compatible with CILS experiments.

TABLE III. Dipole-quadrupole and dipole-octopole polarizabilities ($A$ and $E$, respectively) of $CH_4$. Experimental values are deduced from the comparison of experimental data with theoretical spectra computed by using several potentials.

| Method | Potential | $\|A\|$ (Å$^4$) | $\|E\|$ (Å$^5$) | Reference |
|---|---|---|---|---|
| Theory | | | | |
| *ab initio* (CI) | | 0.74 | 0.76 | [37] |
| *ab initio* (SCF) | | 0.76 | 0.81 | [38] |
| *ab initio* (RPA) | | 0.81 | 0.84 | [39] |
| *ab initio* (CCSD (T)) | | 0.71 | 0.78 | [28] |
| Experiment | | | | |
| proton spin relaxation | | 0.89 | | [40] |
| anisotropic CILS | RMK [33] | 0.75 | 2.7 | [4,5] |
| isotropic CILS | LJ [32] | $0.69\pm0.09$ | $\leqslant1.34$ | this work |
| isotropic CILS | RMK [33] | $0.61\pm0.09$ | $\leqslant1.16$ | this work |
| isotropic CILS | PA [26] | $0.66\pm0.08$ | $\leqslant1.26$ | this work |
| best/recommended | | $0.7^{+0.1}_{-0.2}$ | $0.6\pm0.6$ | this work |

Besides, we checked for every potential that the zero-order moment $M_0^F$ associated with the integrated intensity of the calculated free-dimer DID contribution to the anisotropic spectrum is close to the expected theoretical moment $(1-x_{ani})M_{0,\beta}^{th}$. The same procedure has been adopted for the isotropic spectrum [where $\beta(r)$ is replaced by the second-order DID trace $\alpha(r)=4\alpha_0^3/r^6$].

In Fig. 3 (PA potential), the DID theoretical contribution fits well the experimental data below 150 cm$^{-1}$. Beyond 200 cm$^{-1}$, rototranslational contributions are predominant but some lack of theoretical intensity can be noticed [35]. On the other hand, in Fig. 4 (PA potential), very good agreement exists between theory and experiment in the whole frequency range. The isotropic spectrum thus appears mainly as resulting from the dipole-quadrupole mechanism, although some influence of the dipole-octopole mechanism is visible beyond 500 cm$^{-1}$. It is to be underlined that no fitting procedure has been used here. Such a procedure would not change significantly the global agreement between theory and experiment. For example, a better fit of experimental and theoretical anisotropic spectra can be obtained by increasing the value $A$ of the DQ polarizability. Nevertheless, it would lead to a lesser fit of experimental and theoretical isotropic spectra (making theoretical isotropic intensities due to the DQ polarizability bigger than experimental isotropic intensities). Indeed, the lack of theoretical anisotropic intensity must be attributed to contributions which are not (or not enough) taken into account in our model. Required additional intensities originate from mechanisms associated with the anisotropic spectrum only and/or for which $A$ and $E$ are not the only adjustable parameters (unlike DQ, DO, and CT contributions). First, the strong translational contribution to the anisotropic spectrum is not known with perfect accuracy. Indeed, besides DID, it may be influenced by short-range effects like overlap and exchange. They are not well known in the case of $CH_4$ and are not considered in this work. However, such effects generally lessen intensities and therefore cannot explain alone the discrepancy observed. On the other hand, a bigger NL

contribution (more or less as intense as the DO and CT contributions in Fig. 3) could fill the lack of intensity in the 250–700 $cm^{-1}$ frequency range. The NL contribution reported in Fig. 3 has been computed by using *ab initio* values of molecular parameters obtained by Maroulis [28,29]. However, (i) these *ab initio* values are static values whereas values at laser frequency would have been preferable. (ii) The values of hyperpolarizabilities and multipole moments involved in the NL contribution do not take into account electron correlation corrections [29] (unlike the values of $A$ and $E$ "recommended" in Ref. [28]). (iii) The highest-frequency part of the collision-induced spectra (beyond 700 $cm^{-1}$) cannot be fitted by any of our various theoretical contributions. A similar observation has been done for other globular molecules [9,16]. These remarks point out the validity limits of our model at the highest frequencies. Finally, the contributions of dipole-multipole polarizabilities to the anisotropic spectrum are not easy to measure. This may explain, at least partly, the overestimation of $E$ (relative to Maroulis's *ab initio* corresponding value) made in previous papers [4,5] centered on the analysis of the anisotropic spectrum alone, but at different temperatures (see Table III). Concerning the isotropic spectrum, the DID contribution is of second order and the NL contributions are not to be considered, contrary to the anisotropic spectrum. In this case, dipole-multipole mechanisms are predominant and a "best fitting" procedure may be used in order to evaluate $A$ and $E$ at laser frequency for the various intermolecular potentials. However, considering the size of the experimental error bars for the isotropic spectrum and the mutual competition between DQ and DO mechanisms, it is preferable to determine the ensemble of the solutions $(A,E)$ for which the theoretical isotropic spectrum lies inside the experimental error bars. This can be carried out by using the set inversion method previously described [36]. In Fig. 5, the area formed by the solutions $(A,E)$ is given for the three selected potentials (LJ, RMK, and PA). In Table III, the values $(A,E)$ deduced from Fig. 5 are also presented, together with their uncertainties. The choice of the potential does not change significantly the shapes of the theoretical spectra although it affects slightly the values of $(A,E)$. However, the values of the dipole-multipole polarizabilities at laser frequency are rather close to the static values calculated by Maroulis [28] whatever the potential is. Considering the uncertainties of our data and those connected with the choice of the potential, we recommend for $CH_4$ the

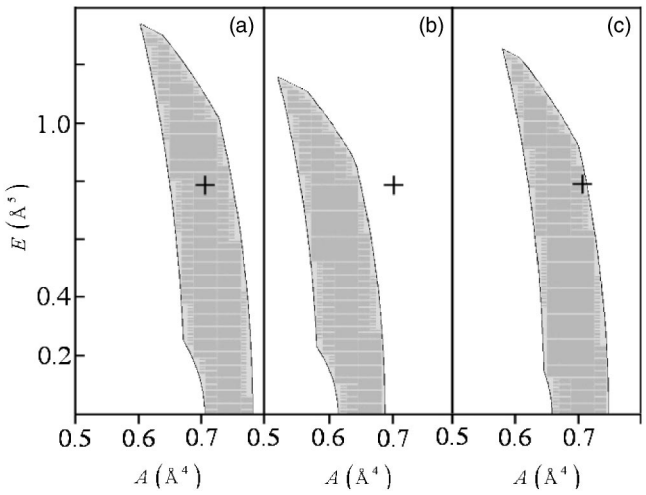


FIG. 5. Area $(A,E)$ of solutions for the dipole-quadripole and dipole octopole polarizabilities. Values of $A$ and $E$ consistent with our experimental data and their error bars lay inside the grey zones. These results are obtained from a set inversion analysis [36] using the comparison of experimental data with isotropic Rayleigh spectra calculated with three potentials: (a) LJ [32], (b) RMK [33], and (c) PA [26]. The cross (+) shows the values computed by Maroulis and used in Figs. 3 and 4 ($A=0.71$ Å$^4$ and $E=0.78$ Å$^5$) [28].

"experimental" evaluations $A=0.7^{+0.1}_{-0.2}$ Å$^4$ and $|E|=0.6\pm0.6$ Å$^5$. They are compatible with the aforementioned *ab initio* computed values of Maroulis [28].

In conclusion, from this work it is shown that multipolar polarizabilities contribute significantly to both the isotropic and anisotropic scattering intensities of gaseous methane at high-frequency shifts. However, although values of dipole-quadrupole and dipole-octopole polarizabilities $(A,E)$ may be evaluated from anisotropic scattering data, the analysis of the isotropic CIS spectrum reported around the Rayleigh line is at the present time the most accurate method to measure high-order multipolar polarizabilities of methane (in particular when using the set inversion technique). This result corroborates the works previously carried out for other optically isotropic molecules, $CF_4$ [8] and $SF_6$ [9].

## ACKNOWLEDGMENT

We wish to thank Pr. N. Meinander for sending us values of the experimental anisotropic binary intensities reported in Ref. [4].

[1] *Phenomena Induced by Intermolecular Interactions*, edited by G. Birnbaum, Vol. 127 of *NATO Advanced Study Institutes, Series B: Physics* (Plenum, New York, 1985).
[2] *Collision- and Interaction-Induced Spectroscopy*, edited by G. C. Tabisz and M. N. Neuman, Vol. 452 of *NATO Advanced Study Institutes Series C: Mathematical and Physical Sciences* (Kluwer Academic, Dordrecht, 1995).
[3] C. G. Gray and K. E. Gubbins, *Theory of Molecular Fluids* (Clarendon Press, Oxford, 1984), Vol. 1.
[4] F. Barocchi, A. Guasti, M. Zoppi, S. M. El-Sheikh, G. C. Tabisz, and N. Meinander, Phys. Rev. A **39**, 4537 (1989).
[5] N. Meinander, G. C. Tabisz, F. Barocchi, and M. Zopii, Mol. Phys. **89**, 521 (1996).
[6] S. Kielich, Proc.-Indian Acad. Sci., Chem. Sci. **94**, 403 (1985).
[7] A. D. Buckingham and G. C. Tabisz, Mol. Phys. **36**, 583 (1978).
[8] A. Elliasmine, J.-L. Godet, Y. Le Duff, and T. Bancewicz, Phys. Rev. A **55**, 4230 (1997).
[9] K. Nowicka, T. Bancewicz, J.-L. Godet, Y. Le Duff, and F. Rachet, Mol. Phys. **101**, 389 (2003).

[10] A. D. Buckingham, Adv. Chem. Phys. **12**, 107 (1967).
[11] C. G. Gray and B. W. N. Lo, Chem. Phys. **14**, 73 (1976).
[12] W. A. Steele, Mol. Phys. **39**, 1411 (1980).
[13] P. Isnard, D. Robert, and L. Galatry, Mol. Phys. **31**, 1798 (1976).
[14] R. Samson and A. Ben-Reuven, J. Chem. Phys. **65**, 3586 (1976).
[15] A. D. Buckingham and G. C. Tabisz, Opt. Lett. **1**, 220 (1977).
[16] A. Elliasmine, J.-L. Godet, Y. Le Duff, and T. Bancewicz, Mol. Phys. **90**, 147 (1997).
[17] Y. Le Duff, J.-L. Godet, T. Bancewicz, and K. Nowicka, J. Chem. Phys. **118**, 11 009 (2003).
[18] R. G. Gordon, Adv. Magn. Reson. **3**, 1 (1968).
[19] T. Bancewicz, Y. Le Duff, and J.-L. Godet, in *Modern Nonlinear Optics*, edited by M. Evans, Advances in Chemical Physics Vol. 119, 2nd ed. (Wiley, New York, 2001), Pt. 1.
[20] J. H. Dymond and E. B. Smith, *The Virial Coefficient of Gases* (Clarendon Press, Oxford, 1969).
[21] C. Adjouri, A. Elliasmine, and Y. Le Duff, Spectroscopy (Eugene, Or.) **11**, 45 (1996).
[22] The scattering plane is defined by the direction of the laser beam and the axis of the collection cone for the scattered beam.
[23] F. Chapeau-Blondeau, V. Teboul, J. Berrué, and Y. Le Duff, Phys. Lett. A **173**, 153 (1993).
[24] T. Bancewicz, Chem. Phys. Lett. **244**, 305 (1995).
[25] J. Downs, K. E. Gubbins, S. Murad, and C. G. Gray, Mol. Phys. **37**, 129 (1979).
[26] B. J. Palmer and J. L. Anchell, J. Phys. Chem. **99**, 12 239 (1995).
[27] N. Meinander, A. R. Penner, U. Bafile, F. Barocchi, M. Zoppi, D. P. Shelton, and G. C. Tabisz, Mol. Phys. **54**, 493 (1985).
[28] G. Maroulis, J. Chem. Phys. **105**, 8467 (1996).
[29] G. Maroulis, Chem. Phys. Lett. **226**, 420 (1994).
[30] N. Meinander, J. Chem. Phys. **99**, 8654 (1993).
[31] H. B. Levine, J. Chem. Phys. **56**, 2455 (1972).
[32] J. O. Hirschfelder, C. F. Curtis, R. B. Bird, *Molecular Theory of Gases and Liquid* (Wiley, New York, 1954).
[33] N. Meinander and G. C. Tabisz, J. Chem. Phys. **79**, 416 (1983).
[34] N. Meinander, G. C. Tabisz, and M. Zoppi, J. Chem. Phys. **84**, 3005 (1986).
[35] We have checked that second-order and higher-order DID's increase by a few percent the DID contribution and so can account for some of the discrepancy between calculation and theory in particular at higher frequencies. However, the consideration of these high-order DID interactions does not change significantly the conclusion of our analysis.
[36] L. Jaulin, J.-L. Godet, E. Walter, A. Elliasmine, and Y. Le Duff, J. Phys. A **30**, 7733 (1997).
[37] R. D. Amos, Mol. Phys. **38**, 33 (1979).
[38] G. H. F. Diercksen and A. J. Sadlej, Chem. Phys. Lett. **114**, 187 (1985).
[39] P. W. Fowler, P. Lazzeretti, and R. Zanasi, Mol. Phys. **68**, 853 (1989).
[40] U. Buck, J. Schleusener, D. J. Malick, and D. Secrest, J. Chem. Phys. **74**, 1707 (1981).